The role of refocusing in dynamic X-wave formation during femtosecond laser filamentation in water

Junjie Xu (徐俊杰)[1], Han Xu (徐 晗)[1], Hui Xiong (熊 辉)[1], Ya Cheng (程 亚)[1*], Zhizhan Xu (徐至展)[1], Weiwei Liu (刘伟伟)[2], and See Leang Chin (陈瑞良)[3]

[1]*State Key Laboratory of High Field Laser Physics, Shanghai Institute of Optics and Fine Mechanics, Chinese Academy of Sciences, Shanghai 201800, China*

[2]*Key Laboratory of Opto-Electronic Information Science and Technology, Ministry of Education, Institute of Modern Optics, Nankai University, Tianjin 300071, China*

[3]*Centre d'Optique, Photonique er Laser (COPL) and Département de Physique, de Génie Physique et d'Optique, Université Laval, Québec, Québec G1K 7P4, Canada*

[*]*E-mail: ycheng-45277@hotmail.com*

Received April 13, 2009

With the evolution of a laser pulse in water, the formation of a nonlinear X wave during femtosecond filamentation is investigated based on numerical simulations. In particular, we analyze the far-field angularly resolved spectra obtained for different temporal portions of the ultrashort pulse during its propagation. Our result shows that the refocusing of ultrashort pulse leads to the formation of dynamic X wave which essentially manifests itself as conical emission.

OCIS codes: 320.0320, 190.5530, 070.4790.
doi: 10.3788/COL20100802.0244.

Femtosecond filamentation in transparent optical media has attracted broad attention for more than one decade[1−11]. From a fundamental point of view, filamentation dynamics constitutes a remarkable system in which many physical effects and properties are observed. It is also particularly attractive for fruitful applications, such as pulse compression[12], supercontinuum generation[13], third harmonic generation[14,15] and remote sensing[16], etc. The major physics of filamentation was proposed as a dynamic competition among Kerr-induced self-focusing and plasma-induced defocusing. It has been pointed out that one signature of filamentation is the X-wave generation in normally dispersive media[17]. Nonlinear X waves (shown as X-shaped light bullets[18,19] in normal dispersive quadratic nonlinear media), which also appear in experiment as conical emissions, are introduced as the stationary wave packets propagating without undergoing the natural spreading due to diffraction or dispersion over long distances, and exhibiting a conical energy flux with X-shaped intensity distribution both in the near field (space-time domain) and in the far field (wave-number-frequency domain). In fact, the early manifestation of the X-shaped intensity structures in both space-time domain and wave number-frequency domain was studied in detail in Refs. [2] and [4] in three-dimensional (3D) plots from the point of view of the physics of conical emission, although the word "X-wave" was not used at that time. Afterwards, intensive experimental and theoretical studies have been performed to study the same problem from the point of view of X-wave formation in various media[20−23]. In most of these studies, angularly resolved spectra of the entire pulses, which are either measured experimentally or calculated theoretically, frequently show X-shaped structures. In this letter, we show that by performing angularly resolved spectral analyses on different temporal portions of an ultrashort pulse during its nonlinear propagation in water, new light can be shed on the dynamics of X-wave formation or conical emission which has not yet been revealed so far.

With simulations of a (3+1)-dimensional model, we study the femtosecond filamentation in water for the purpose of gaining deeper insight into the dynamics of X-wave formation. The theoretical model is based on an extended nonlinear Schrödinger (NLS) equation governing the slowly varying envelope of a linearly polarized laser electric field, coupled with an evolution equation for the electron density generated by ionization. The equations can be written as

$$\frac{\partial \varepsilon}{\partial z} = \frac{\mathrm{i}}{2k}\Delta_{\perp}\varepsilon - \mathrm{i}\frac{k''}{2}\frac{\partial^2 \varepsilon}{\partial t^2} + \mathrm{i}k_0 n_2 |\varepsilon|^2 \varepsilon - \frac{\sigma}{2}(1+\mathrm{i}\omega\tau_{\mathrm{c}})\rho\varepsilon - \frac{\beta_K}{2}\left(1-\frac{\rho}{\rho_{\mathrm{at}}}\right)|\varepsilon|^{2K-2}\varepsilon, \quad (1)$$

$$\frac{\partial \rho}{\partial t} = \sigma_K(\rho_{\mathrm{at}}-\rho)|\varepsilon|^{2K} + \frac{\sigma}{U_{\mathrm{i}}}\rho|\varepsilon|^2, \rho \ll \rho_{\mathrm{at}}, \quad (2)$$

where t refers to the retarded time variable $t = \tau - z/v_{\mathrm{g}}$ (τ is the real time and v_{g} is the group velocity), and z denotes propagation distance; $k = n_0\omega_0/c$ and ω_0 are the wave number and frequency of the carrier wave, respectively. The Laplacian operator $\Delta_{\perp} = \frac{\partial^2}{\partial x^2} + \frac{\partial^2}{\partial y^2}$. Parameters including the linear and nonlinear indices of the media n_0 and n_2, the dispersive coefficient k'', the momentum transfer collision time τ_{c}, the number of photons K, the mean ionization potential u_{i}, the multiphoton absorption cross section β_K, and the transition rate σ_K are the same as those in Ref. [20]. In this model, as shown in Eq. (1), the linear effects include the transverse diffraction and group-velocity dispersion, and the

nonlinear effects include the optical Kerr effect, plasma absorption, plasma defocusing, and multiphoton absorption, whereas in Eq. (2) the density ρ of the electron plasma is generated by multiphoton ionization and partial cascade ionization[24]. The quantity $\rho_{\rm at}$ denotes the density of neutral molecules of water. Since the shock-term in a more comprehensive theoretical model beyond the slowly varying envelop approximation only induces quantitative change of the extension of the pulse in the far field without disturbing the major dynamics of the pulse transformation during the filamentation in water[20], it is not taken into account in the present work.

We assume in our simulation that the beam is focused onto the entrance surface of a water cell of about 3-cm length, and its geometric focus, after accounting for the refractive index differences among air, the glass window of the water cell, and water, is assumed to be located in the middle of the water cell (1.5 cm away from the entrance surface). Gaussian beam profiles are employed for the focal spot in both spatial and temporal domains, with a transverse beam waist at the geometric focus, $w_0 = 75$ μm (at $1/e^2$ level), a temporal half width $t_p = 130$ fs (full-width at half-maximum (FWHM) $t_{\rm FWHM} = t_p\sqrt{2\ln 2}$), and an initial pulse energy $E_{\rm in} = 2.2$ μJ. In addition, in our simulation, the nonlinear propagation of the beam starts from the entrance surface; therefore, the envelope of the initial pulse can be described as

$$\varepsilon(x,y,z_0,t) = \sqrt{\frac{2P_{\rm in}}{\pi w_{\rm in}^2}} \exp\left[-\frac{x^2+y^2}{w_{\rm in}^2}\left(1-\frac{{\rm i}kw_{\rm in}^2}{2R_{\rm in}}\right)-\frac{t^2}{t_p^2}\right], \quad (3)$$

where $P_{\rm in} = \sqrt{\pi/2}E_{\rm in}/t_p$ denotes the input power; $w_{\rm in} = w_0\left(1+z_0^2/z_f^2\right)^{1/2}$ and $R_{\rm in} = n_0 z_0(1+z_f^2/z_0^2)$ are the transverse size and the curvature at the initial calculation surface with w_0 being the waist size of the focus, respectively. $z_f = n\pi w_0^2/\lambda$ denotes the Rayleigh length, and $z_0 = -1.5$ cm. The central wavelength of the laser pulse is $\lambda_0 = 800$ nm.

The temporally integrated intensity (i.e., $\int_{-\infty}^{+\infty} I(x,y=0,t){\rm d}t$) of the pulse in x-z plane is shown in Fig. 1(a). The peak intensity of the pulse and the maximum electron density in the filament are shown in Fig. 1(b) as functions of the propagation distance. Owing to the nonlinear Kerr effect, the laser pulse starts to self-focus at $z \simeq -0.8$ cm, significantly before the geometrical focus ($z = 0$ cm). At this position, the ionization and the peak laser intensity simultaneously reach their maxima. In addition, we observe generation of conical emission in Fig. 1(a) which is consistent with previous report[24].

Figure 2 shows the near-field transverse energy flux distribution, the on-axis intensity profile of the pulse during the filamentation, and the far field at a propagating distance of $z = -0.3$ cm. The energy flux in the x direction was obtained by monitoring $1/2{\rm i}\,(\varepsilon^*\partial\varepsilon/\partial x - \varepsilon\partial\varepsilon^*/\partial x)$[21,25,26]. Initially with a Gaussian profile, the pulse splits into leading and trailing pulses in the spatio-temporal dimension asymmetrically after propagating a distance of $z = -0.3$ cm, as can be clearly seen in Fig. 2(a)[20]. In addition, a typical X-shaped wave which is composed of two half X branches[6] starts to appear in the angular spectrum, as shown in Fig. 2(b). One should have also noticed that in Fig. 2(a), the energy fluxes corresponding to both the leading and trailing parts show a pair of inward and outward fluxes (see, for example, the energy fluxes in the temporal windows A and B form a pair of fluxes in the leading part; while the energy fluxes in the temporal windows C and D form the other pair of fluxes in the trailing part of the pulse), which is similar to the previous results[21,22,25–27]. In order to extract the information of angular spectrum which corresponds to each inward and outward flux, we calculate the angular spectrum of the pulse within four temporal windows, as indicated by the windows A, B, C, and D in Fig. 2(a). The temporal windows A, B, C, and D are designed to match the temporal width of the inward and outward fluxes of the leading and trailing pulses, respectively.

The angular spectra of the pulse within the four temporal windows are shown in Figs. 2(c)–(f). It is displayed clearly that the ranges B and C, namely the outward energy fluxes, have distinct half-X-shape far fields, as shown in Figs. 2(d) and (e), whereas far fields of the inward energy flux seem to remain Gaussian shape, as shown in Figs. 2(c) and (f). Although the result presented here is calculated based on a specific input power, similar results have been observed at other input peak powers (e.g., $P_{\rm in} = 3P_{\rm cr}$, where $P_{\rm cr}$ is the critical power) in our simulations. One therefore might draw the conclusion that the outward energy flux plays a major role for an X-wave generation during its incipient stage.

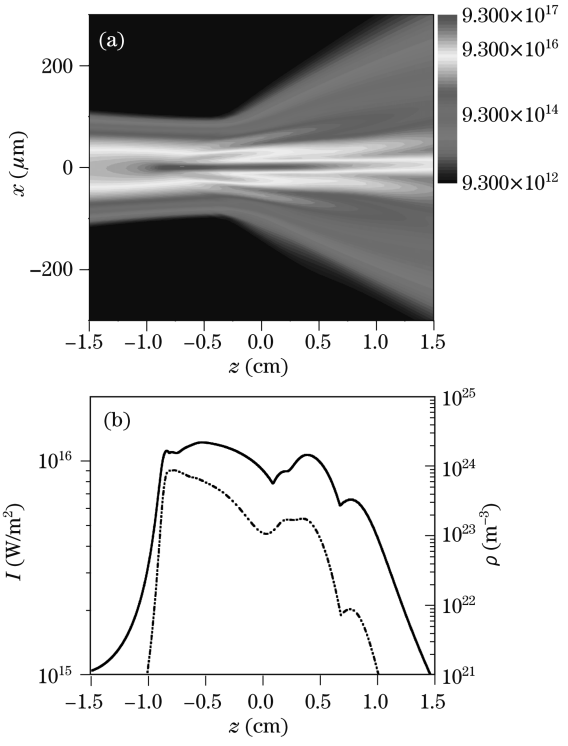

Fig. 1. (a) Intensity distribution of the laser beam in the x-z plane; (b) peak intensity I (solid line) and electron density ρ (dotted line) versus laser pulse propagation distance z. The intensity levels are plotted in logarithmic scale.

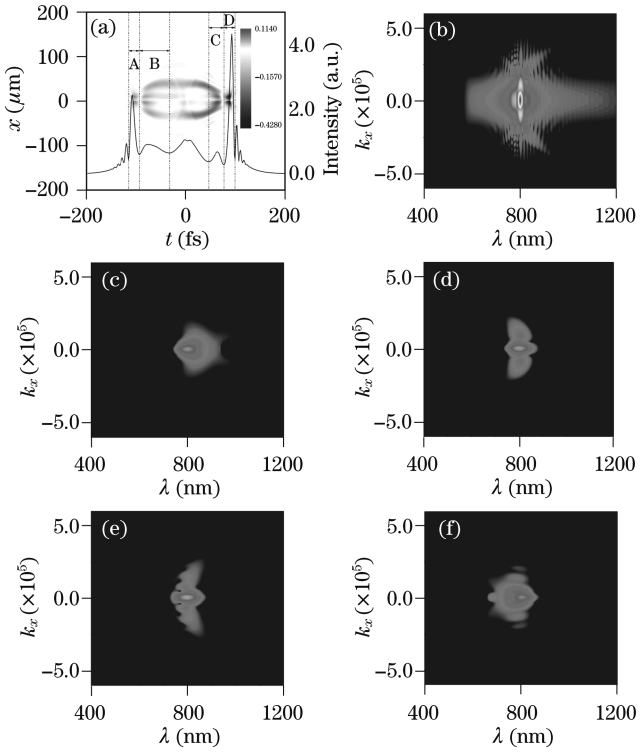

Fig. 2. (a) Transverse energy flux distribution (in normalized units), including inward (windows A and D) and outward fluxes (windows B and C) and the on-axis intensity profile of the pulse; (b) far field for the whole electric field; (c)–(f) far fields for four temporal windows (A, B, C, and D) of energy flux at the propagation distance of $z = -0.3$ cm.

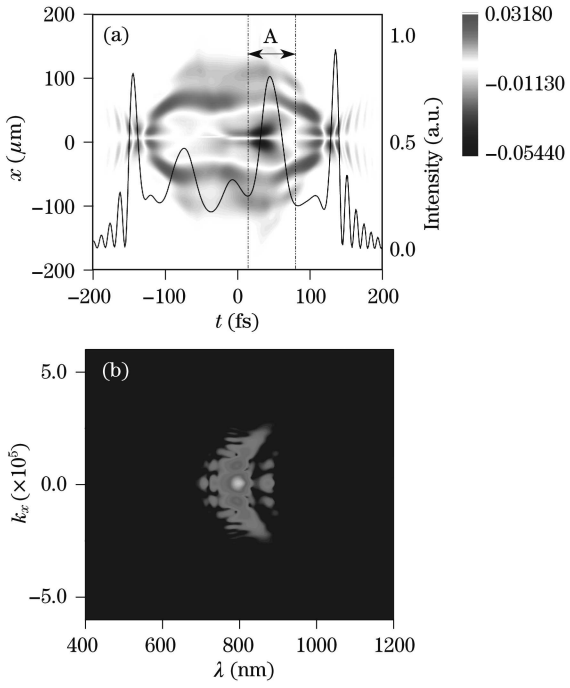

Fig. 3. (a) Transverse energy flux distribution (in normalized units) and (b) far field for the temporal window of energy flux at the propagation distance of $z = 0.3$ cm.

Recently, it has been suggested that the formation of X wave could facilitate an extended propagation distance in which the laser pulse could maintain tightly focused and therefore, a high peak intensity[22]. The above-mentioned two X waves belonging to the leading and trailing parts of the pulse, nevertheless, will not be able to keep the pulse filamentation over a distance far beyond the Rayleigh range because both X waves feature an outward energy flux which cannot refill the energy into the filament. The mechanism of the formation of the X wave at this stage could be understood as follows. When the femtosecond filamentation occurs, it is usually accompanied by localized plasma formation and refractive index change of the un-ionized gas medium within the filament, by which the broad-spectrum light in the filament can be scattered out to form conical emission. In turn, the scattered white light can serve as seeds for various nonlinear frequency conversion processes and will be efficiently amplified with the largest gain if the phase-matching condition for three-wave mixing can be fulfilled, which leads to the formation of the conical emission[13,17].

We would like to point out here that only the repetitive cycle of conical emission and refocusing of the conical emission, which indeed give rise to the inward energy flux, can support the extended propagation distance of filamentation. In this case, the outer region of the conical emission can serve as the energy reservoir[28] to compensate the energy loss in the filament during propagation. In order to search for such a conical emission, we propagate the femtosecond pulse farther in water. Figure 3 shows the near-field transverse energy flux distribution, the on-axis intensity profile of the pulse during the filamentation, and the far field at a propagating distance of $z = 0.3$ cm. Interestingly enough, it can be seen in Fig. 3(a) that near the time $t = 0$, a new inward flux emerges near the propagation axis together with the outward flux around it. Again, we apply a temporal window (window A in Fig. 3(a)) which temporally matches the newly generated inward energy flux so that its angular spectrum can be obtained. Remarkably, the angular spectrum in Fig. 3(b) clearly shows an X-shaped structure, indicating the formation of an X wave with an inward energy flux. The physics behind this seems to be that there are both inward and outward flowing fluxes that balance each other approximately. In principle, such a conical emission should be able to support a prolonged optical guiding of high intensity with a distance significantly longer than the Rayleigh range[21].

In conclusion, we numerically investigate the filamentation of an ultrashort pulse in water by studying the far-field and near-field transverse energy fluxes during the evolution with the propagating distance. We observe that at the early stage of filamentation, only half-X waves featuring with outward energy flux are formed, which, however, cannot serve as an energy reservoir for extending the filament length. Further propagation of the pulse leads to refocusing of beam and creates an X wave with inward energy flux. The newly born X wave plays an important role in the following propagation of filamentation pulse.

This work was supported by the National Basic Research Program of China (No. 2006CB806000). Y. Cheng acknowledges the supports of the 100 Talents Program of the Chinese Academy of Sciences, the Shanghai Pujiang Program, and the National Outstanding Youth Foundation. W. Liu acknowledges the sup-

ports of the National Basic Research Program of China (No. 2007CB310403) and the National Natural Science Foundation of China (No. 10804056). S. L. Chin acknowledges the support of the Canada Research Chairs Program.

References

1. M. Mlejnek, E. M. Wright, and J. V. Moloney, Opt. Lett. **23,** 382 (1998).
2. I. S. Golubtsov, V. P. Kandidov, and O. G. Kosareva, Atmos. Oceanic Opt. **14,** 303 (2001).
3. V. P. Kandidov, O. G. Kosareva, I. S. Golubtsov, W. Liu, A. Becker, N. Akozbek, C. M. Bowden, and S. L. Chin, Appl. Phys. B **77,** 149 (2003).
4. V. P. Kandidov, I. S. Golubtsov, and O. G. Kosareva, Quantum Electron. **34,** 348 (2004).
5. T.-T. Xi, X. Lu, and J. Zhang, Phys. Rev. Lett. **96,** 025003 (2006).
6. A. Couairon and A. Mysyrowicz, Phys. Rep. **441,** 47 (2007).
7. L. Bergé, S. Skupin, R. Nuter, J. Kasparian, and J. P. Wolf, Rep. Prog. Phys. **70,** 1633 (2007).
8. J. Kasparian and J. P. Wolf, Opt. Express **16,** 466 (2008).
9. S. L. Chin, S. A. Hosseini, W. Liu, Q. Luo, F. Théberge, N. Aközbek, A. Becker, V. P. Kandidov, O. G. Kosareva, and H. Schroeder, Can. J. Phys. **83,** 863 (2005).
10. H. Sun, F. He, J. Xu, Y. Liao, Y. Cheng, Z. Xu, X. Jiang, and Y. Dai, Chin. Opt. Lett. **7,** 329 (2009).
11. Y. Zhang, Y. Chen, Z. Li, S. Xu, W. Liu, and S. L. Chin, Acta Opt. Sin. (in Chinese) **29,** 781 (2009).
12. C. P. Hauri, W. Kornelis, F. W. Heling, A. Heinrich, A. Couairon, A. Mysyrowicz, J. Biegert, and U. Keller, Appl. Phys. B **79,** 673 (2004).
13. M. Kolesik, E. M. Wright, and J. V. Moloney, Opt. Lett. **32,** 2816 (2007).
14. H. Xu, H. Xiong, R. Li, Y. Cheng, Z. Xu, and S. L. Chin, Appl. Phys. Lett. **92,** 011111 (2008).
15. H. Xiong, H. Xu, Y. Fu, Y. Cheng, Z. Xu, and S. L. Chin, Phys. Rev. A **77,** 043802 (2008).
16. J. Kasparian, M. Rodriguez, G. Méjean, J. Yu, E. Salmon, H. Wille, R. Bourayou, S. Frey, Y.-B. André, A. Mysyrowicz, R. Sauerbrey, J.-P. Wolf, and L. Wöste, Science **301,** 61 (2003).
17. M. Kolesik, E. M. Wright, and J. V. Moloney, Phys. Rev. Lett. **92,** 253901 (2004).
18. H. Xu and H. Zeng, Opt. Lett. **32,** 1944 (2007).
19. H. Xu and H. Zeng, Opt. Lett. **32,** 820 (2007).
20. A. Couairon, E. Gaižauskas, D. Faccio, A. Dubietis, and P. Di Trapani, Phys. Rev. E **73,** 016608 (2006).
21. D. Faccio, A. Averchi, A. Lotti, P. Di Trapani, A. Couairon, D. Papazoglou, and S. Tzortzakis, Opt. Express **16,** 1565 (2008).
22. D. Faccio, A. Matijosius, A. Averchi, A. Lotti, O. Jedrkiewicz, A. Dubietis, G. Tamosauskas, A. Couairon, F. Bragheri, D. Papazoglou, S. Tzortzakis, and P. Di Trapani, Phys. Rev. A **78,** 033826 (2008).
23. D. Faccio, A. Averchi, A. Couairon, M. Kolesik, J. V. Moloney, A. Dubietis, G. Tamosauskas, P. Polesana, A. Piskarskas, and P. Di Trapani, Opt. Express **15,** 13077 (2007).
24. S. L. Chin, F. Theberge, and W. Liu, Appl. Phys. B **86,** 477 (2007).
25. P. Polesana, M. Franco, A. Couairon, D. Faccio, and P. Di Trapani, Phys. Rev. A **77,** 043814 (2008).
26. D. Faccio, A. Lotti, A. Matijosius, F. Bragheri, V. Degiorgio, A. Couairon, and P. Di Trapani, Opt. Express **17,** 8193 (2009).
27. F. Bragheri, D. Faccio, A. Couairon, A. Matijosius, G. Tamošauskas, A. Varanavičius, V. Degiorgio, A. Piskarskas, and P. Di Trapani, Phys. Rev. A **76,** 025801 (2007).
28. W. Liu, F. Thérge, E. Arálo, J.-F. Gravel, A. Becker, and S. L. Chin, Opt. Lett. **30,** 2602 (2005).